LASER & PHOTONICS REVIEWS

www.lpr-journal.org

Efficient Emission Outcoupling from Perovskite Lasers into Highly Directional and Long-Propagation-Length Bloch Surface Waves

Kirill R. Safronov, Anna A. Popkova, Daria I. Markina, Anatoly P. Pushkarev, Sergey V. Makarov, Vladimir O. Bessonov, and Andrey A. Fedyanin**

Halide perovskite micro- and nanolasers have become a novel platform for efficient generation of coherent emission in the whole visible range. However, the laser emission outcoupling from the perovskite microcrystals faces a number of problems related to large divergence angle, light-soaking by a substrate, and high losses in the case of coupling with nanowaveguides. Here the perovskite nano- and microlasers are proposed to be integrated with a photonic crystal supporting Bloch surface waves (BSWs), which are coupled directly from the perovskite lasers with the efficiency of over 16%. The BSWs exciting at 535-nm wavelength show high in-plane directivity, down to 9°, and long-propagation length, up to 50 µm. Moreover, a pronounced beam steering effect for the generated laser emission is demonstrated by varying the pumping laser beam position, which provides an additional degree of freedom for in-plane control of the lasing mode outcoupling.

1. Introduction

Modern integrated photonics successfully solves various complex tasks in computing,[1] quantum simulation,[2] nonlinear optics,[3] etc. Particularly, a lot of applications require integrated photonics in the visible.[4,5] In turn, unlocking the full potential of the visible integrated photonics platform can be achieved only through implementation of on-chip nano- and microlasers. One of the best types of semiconductor materials for the ultracompact lasers in the visible range is a family of halide perovskites, which provides low lasing threshold and broadband spectral tunability, as well as allows simple fabrication of small lasers by various cost-efficient approaches.[6–21]

K. R. Safronov, A. A. Popkova, V. O. Bessonov, A. A. Fedyanin
Faculty of Physics
Lomonosov Moscow State University
Moscow 119991, Russia
E-mail: fedyanin@nanolab.phys.msu.ru

D. I. Markina, A. P. Pushkarev, S. V. Makarov
School of Physics and Engineering
ITMO University
St. Petersburg 197101, Russia
E-mail: s.makarov@metalab.ifmo.ru

The ORCID identification number(s) for the author(s) of this article can be found under https://doi.org/10.1002/lpor.202100728

DOI: 10.1002/lpor.202100728

Despite, the platforms for low-loss waveguiding and manipulation at microscale based on such materials as SiO_2,[22] Si_3N_4,[23] diamond,[24] and GaP[25] were demonstrated, their integration with perovskite ultracompact lasers is still a big challenge owing to relatively low efficiency, below 10% level, of lasing mode coupling into a waveguide[26,27] or short propagation length of the coupled light in case of plasmonic nano-waveguides.[28]

In this work, we propose to integrate halide perovskite $CsPbBr_3$ nano- and microlasers with a photonic crystal (PC) supporting Bloch surface waves (BSWs) to achieve highly directional and long-distance propagation of lasing mode emitted with high coupling efficiency. BSW is a dielectric analog of surface plasmon–polariton and has the same unique features such as surface sensitivity and electric field enhancement. However, BSWs are sustained by an all-dielectric PC and its propagation length exceeds that for plasmon–polaritons by several orders of magnitude, especially in the visible range.[29–31] Experimental results on leakage radiation fluorescent micro-spectroscopy and corresponding full-wave numerical simulations allow us to determine all main parameters for the BSWs excited by the perovskite nano- and microlasers. Moreover, the PC, being an open-type isotropic 2D waveguide, provides an additional degree of freedom to control the direction of laser beam propagation by changing optical pumping conditions, pawing the way to multi-directional signal routing with a single integrated light source.

2. Results

2.1. Integration of Perovskite Lasers with Photonic Crystal

The studied system is schematically shown in **Figure 1**a. We use one of the best perovskite compositions ($CsPbBr_3$) for lasing purposes, stably emitting coherent light with low threshold at room temperature[10,11] and which has been previously successfully integrated into PC.[32] Halide perovskite $CsPbBr_3$ nano- and microlasers lie on the surface of 1D PC sustaining TE-polarized BSW (see Methods for details). After the external optical excitation the lasing mode leaves the perovskite and couples with

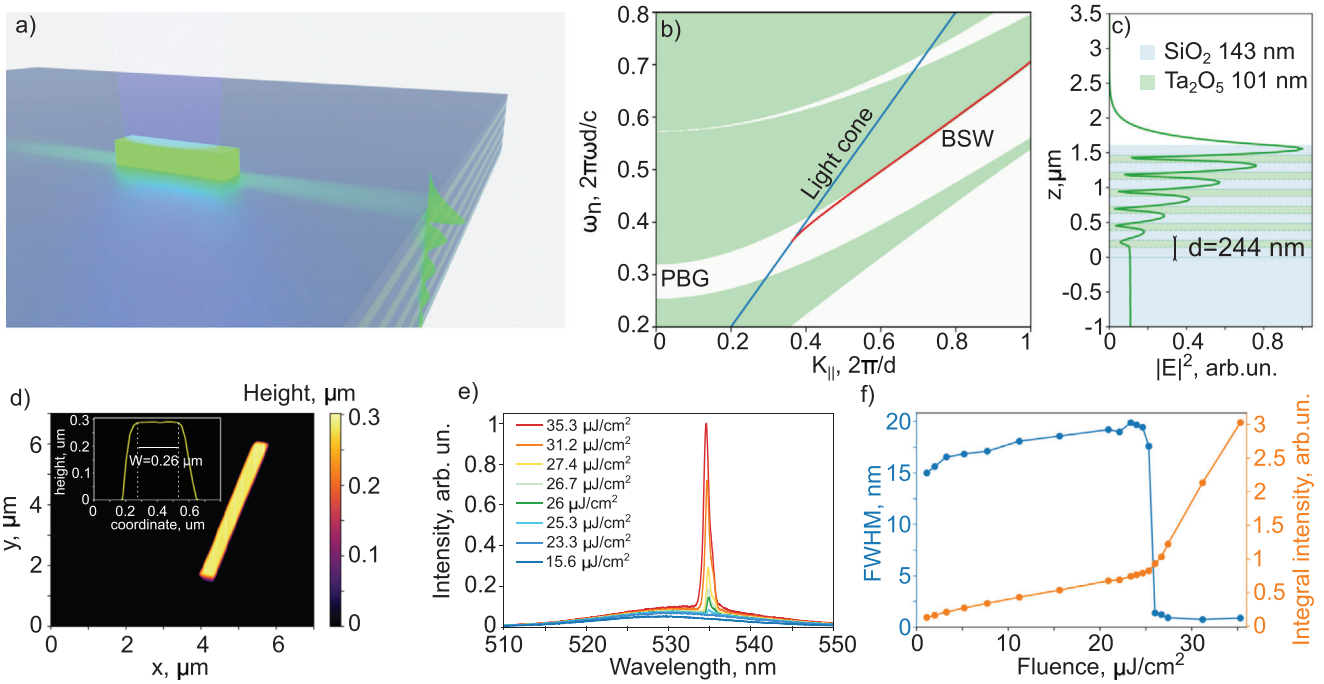

Figure 1. Perovskite nanolaser for excitation of Bloch surface waves. a) Schematic of the experiment on lasing from the perovskite nanowire on the surface of PC. b) Band diagram of studied 1D PC. White regions correspond to forbidden bands (PBG). Blue line depicts vacuum light cone. BSW dispersion is shown with red curve. c) BSW field distribution in the studied PC at $\lambda = 535$ nm. d) AFM image of the $CsPbBr_3$ nanowire on the photonic crystal surface. e) Emission spectra for different values of pump fluence. f) Dependence of the integral emission intensity and FWHM of the emission spectra for the perovskite nanolaser on the excitation fluence.

BSW propagating on a bare PC surface. To realize this design, the PC parameters were optimized for the efficient BSW excitation at the $CsPbBr_3$ luminescence wavelength. Figure 1b shows band diagram of the studied PC. BSW exists outside the light cone and near the edge of photonic bandgap (PBG). Proximity of PBG leads to high BSW leakage rate (see Section S1, Supporting Information), which helps us to study the BSW propagation using leakage radiation microscopy.[33,34] BSW can be excited in a wide range of spectrum from 450 to 650 nm, where effective refractive index n_{BSW}, which is equal to the ratio of BSW propagation constant k_{BSW} and the radiation wavevector in vacuum k_0, decreases from 1.27 to 1. The BSW electric field distribution calculated by the transfer matrix method[35] is shown in Figure 1c. BSW is localized near the PC surface enabling efficient coupling with nanolaser radiation propagating along the PC surface. BSW propagation length L_{BSW} strongly depends on the wavelength and increases from 27 μm at $\lambda = 450$ nm to 344 μm at $\lambda = 650$ nm being around 75 μm in the gain region $\lambda = 530$–540 nm[10,11,17] (see Section S1, Supporting Information).

$CsPbBr_3$ nano- and microlasers were deposited on the surface of PC by drop-casting of perovskite precursor solution at ambient conditions similarly to a procedure reported elsewhere[17] (see Experimental Section for details), resulting in a set of randomly arranged nano- and microwires and, microplates of various sizes. The geometrical parameters of the samples were determined by an atomic force microscope (AFM) working in a semi-contact mode. The AFM image of a nanowire laser studied below is shown in Figure 1d. The nanolaser has subwavelength cross-sectional dimensions, its height is 290 nm and width is 260 nm. The laser length is 4.5 μm.

To study the laser properties of perovskite structures, the sample was irradiated by slightly focused femtosecond light pulses with the wavelength of 400 nm and the repetition rate of 50 kHz (see Section S2, Supporting Information). Figure 1e shows the nanowire luminescence spectra for various pump fluences, where lasing regime is confirmed by the characteristic threshold dependences of the intensity and emission linewidth (Figure 1f). The narrow peak of laser generation is observed near $\lambda = 534$ nm for fluences greater than 24 μJ cm^{-2}, which is close to that of $CsPbBr_3$ nanolasers on ITO substrate (see Section S3, Supporting Information) and consistent with previous studies of perovskite lasers fabricated by the same method.[17,36,37] Thus, our PC preserves the lasing properties of the perovskite lasers, maintaining the quality factor of the emission peak at 750. Depending on the size of the microplates and nanowires, both single-mode and multimode lasing are observed in their emission spectra.

2.2. Properties of Bloch Surface Waves Generated by a Subwavelength Laser

The coupling of perovskite emission with BSW was studied by leakage radiation microscopy, which is schematically shown in **Figure 2**a (see Methods for details). BSW is a leaky mode meaning that part of the BSW energy leaks into the substrate during propagation. Intensity of leakage radiation is proportional to the

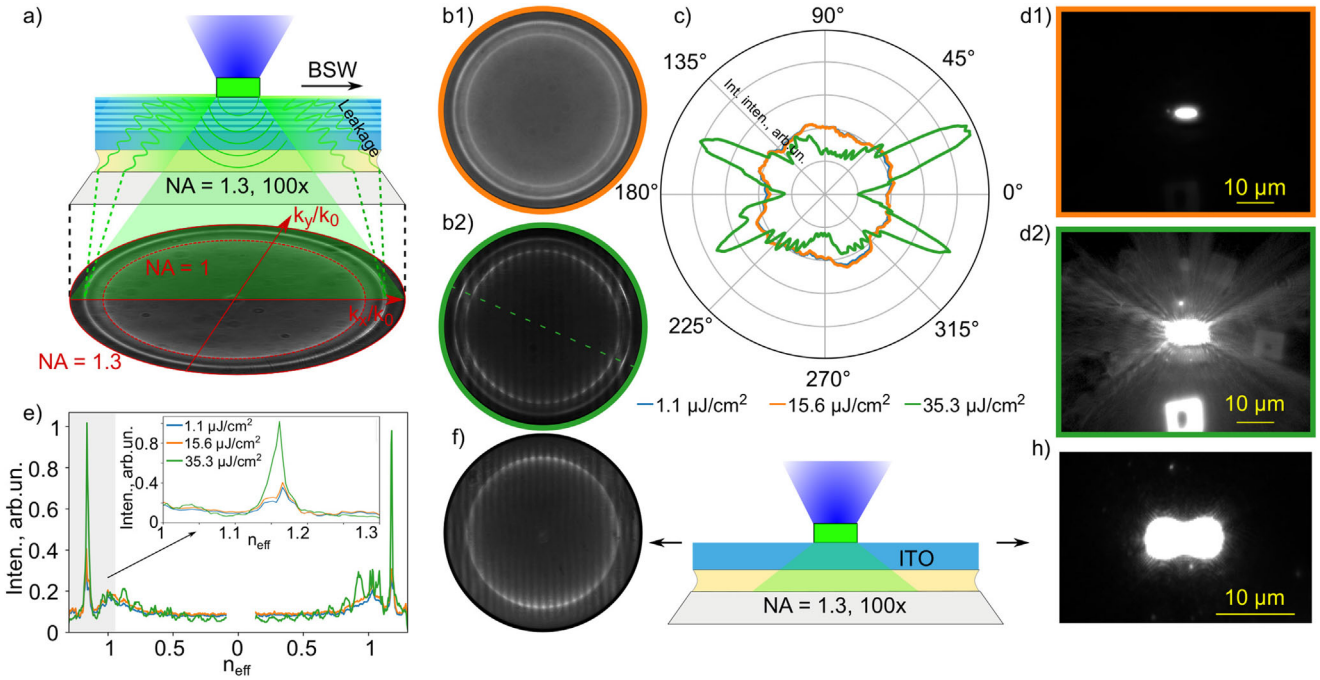

Figure 2. Coupling of perovskite luminescence with Bloch surface waves. a) Schematic of leakage radiation microscopy experiment on coupling of perovskite emission with BSWs. Red circles show numerical aperture of the air cone (NA = 1) and the collecting objective lens (NA = 1.3). b) BFP images of the excited BSW for pump fluence below (b1) and above (b2) lasing threshold. c) Directivity of the perovskite nanowire emission for various pump fluences. d) Visualization of the excited BSW for pump fluence below (d1) and above (d2) the lasing threshold. e) Dependence of intensity in BFP image cross-section (shown with green dashed line in Figure 2 b2) on effective refractive index n_{eff}. Inset shows the dependence for n_{eff} >1 for various pump fluences. f) BFP and h) FFP images of perovskite emission from nanowire on the ITO surface with pump fluence above the lasing threshold.

BSW near-field intensity,[34] while the leakage emission angle α satisfies the phase-matching condition $n_{BSW} = n_{sb}\sin(\alpha)$, where n_{sb} is the refractive index of the substrate. Leakage radiation was collected with an objective lens. We obtained images of both front focal plane (FFP) and back focal plane (BFP). FFP image gives information about BSW near-field distribution, while BFP image shows BSW wavevector distribution. Since PC is isotropic in the surface plane, the BSW in the BFP image forms a circle with the diameter corresponding to the BSW effective refractive index n_{BSW}.[38] Brighter areas of the circle indicate that BSW is more intense in the corresponding directions. Thus, the analysis of the intensity distribution in the circle allowed us to construct the BSW directivity diagram. The BFP images of BSW excited by the perovskite nanowire from Figure 1d are shown in Figure 2b. Below lasing threshold (Figure 2 b1) BSW excitation is uniform in all directions with n_{BSW} ranging from 1.14 to 1.2. As the pump fluence is increased to above-threshold values, BFP image dramatically changes (Figure 2 b2). First of all, fringes across the image are observed due to interference of radiation coming out of nanowire end facets.[39] Second, BSW excitation directivity becomes more pronounced. We estimated radiation directivity from BFP image as the sum of the signal corresponding to the BSW circle for different azimuthal angles normalized to the total circle intensity (see Figure 2c). Four directions become pronounced when the pump fluence exceeds laser threshold. The direction of BSW excitation is also visualized through FFP image of the sample surface. We were able to detect only propagating modes with $n_{eff} > 1$ using the BFP filtration (see Section S2, Supporting Information). Figure 2d shows the FFP images of the nanowire below (d1) and above (d2) the lasing threshold. No directivity is observed at the prethreshold fluence values. For the above-threshold ones, there is a pronounced increase in intensity from the wire corners, corresponding to the directivity obtained from the BFP images analysis. Appearance of BSW directivity is also accompanied by the narrowing of n_{BSW} distribution (Figure 2e).

We used perovskite structures deposited on the ITO surface as the reference sample. The homogeneous substrate does not support any propagating mode and BFP images are featureless except interference fringes from nanowire end facets (Figure 2f). The directivity is uniform for all values of pump fluence. We observed quasi-uniform intensity for pump fluence below the threshold and brightly glowing ends of the nanowire for the fluences above (Figure 2h and Figure S3d, Supporting Information).

The directional BSW excitation by perovskite structures was numerically studied with the finite difference in the time domain (FDTD) method in the Lumerical Solution software. First, we calculated modes sustained by the nanowire in the luminescence wavelength range (520–540 nm). Nanowire was modeled as rectangular parallelepiped with geometric parameters obtained from the experiment (Figure 1d). During calculations, the perovskite material was considered to be lossless with refractive index of 2.5,[10] which corresponds to lasing regime. A cloud of dipoles with random phases and dipole moments parallel to TE polarization (i.e., parallel to PC surface and perpendicular to long side of the nanowire) was placed inside the perovskite structure. We calculated time dependence of field amplitude inside the wire and

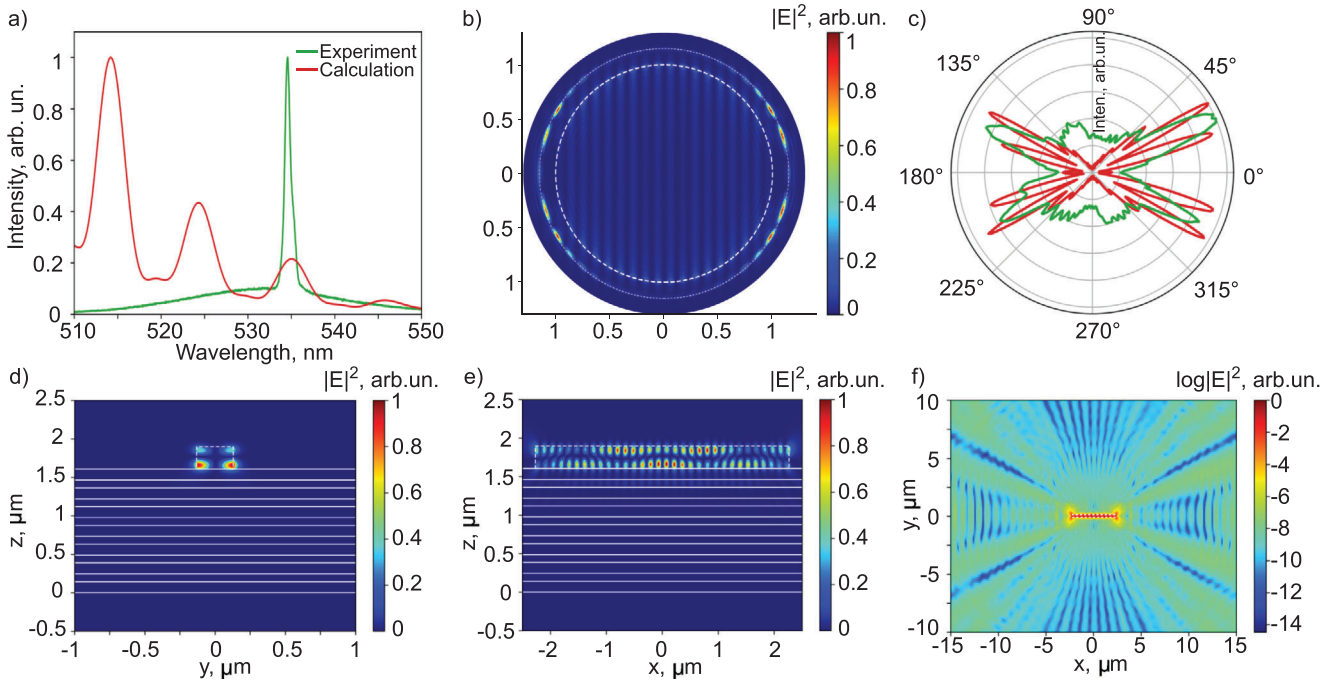

Figure 3. Simulation of perovskite laser radiation coupling with BSW. a) Calculated spectrum of modes supported by the nanowire (red curve) and measured emission spectrum of the nanowire (green curve). b) Calculated BFP image at $\lambda = 535$ nm. Inner dashed circle corresponds to $n_{\text{eff}} = 1$, outer circle – to $n_{\text{eff}} = n_{\text{BSW}} = 1.15$. c) Comparison of calculated (red curve) and measured (green curve) directivity of nanolaser radiation at $\lambda = 535$ nm. d) Field distribution across the perovskite nanowire at $x = 0$. Nanowire edges are shown with white dashed line, PC layers—with solid white lines. e) Field distribution along the nanowire (xz plane) at $y = 0$. f) Logarithm of field distribution along the nanowire (xy plane) at $z = 1.6$ μm.

obtained the spectrum of radiation (**Figure 3**a). Three modes are observed inside the luminescence band, while only one of them, at $\lambda \approx 535$ nm, falls within the gain region of 530–540 nm. Calculated and measured spectral positions of the mode are almost coincide with a slight difference most likely caused by a small deviation of parameters of the simulated nanowire from the real ones. Dependence of the mode spectrum on the nanowire parameters is given in Section S4, Supporting Information. The measured spectrum of the lasing mode is narrower than the calculation predicts since spectral width of laser line is narrower than width of the resonance mode in cavity formed by the nanowire facets. This effect in perovskite lasers is discussed in detail in ref. [36]. We computed the corresponding BFP image for 535-nm wavelength (Figure 3b). Similarly to measured BFP image, interference fringes and excitation of BSW (bright spots outside of $n_{\text{eff}} = 1$ circle) are observed. The directivity of nanowire radiation was obtained from BFP image in the same manner as for experimental one. Calculated directivity agrees well with experimentally measured one (Figure 3c), but instead of four lobes we observed eight lobes. The latter is a consequence of the presence in the experiment of several other effects that contribute to the formation of the BFP image. First of all, in the experiment we collect all radiation with wavelengths greater than 495 nm meaning that the observed BFP image is a superposition of coherent laser radiation and incoherent spontaneous emission, which is not taken into account in the calculations. Second, the BFP image is formed by the radiation collected from the full field of view of the oil-immersion objective lens which has a diameter of 265 μm. It means that the nanowire surrounding affects the BFP image. As the lasers were created by a wet-chemistry process leading to randomly arranged perovskite structures, the nanowire is always surrounded by small perovskite particles and other lasers that scatter propagating BSW and contribute to smoothing of the directivity pattern. Figure 3b shows that bright areas of the BSW circle in the BFP image are observed in the intersection of the interference fringes and BSW circle, indicating the interference nature of the BSW directivity pattern. In the case of a wire with a subwavelength cross section, its end facets act as BSW point sources, forming an interference pattern on the PC surface similar to Young's interference experiment (see Section S5, Supporting Information). As a result, the BSW directivity is governed only by the nanowire length and can be easily predicted in advance based on size measurements.

The excited mode of the nanowire was studied in more detail. Cross-section of field distribution across the structure is shown in Figure 3d. The distribution has two maxima along each of the axes y and z corresponding to the field component E_z, while E_y component has single maximum along the axis y (see Section S4, Supporting Information for more details). Cross-section of field distribution along the structure is shown in Figure 3e with clear Fabry–Perot cavity mode. Figure 3f shows field distribution in a cross-section parallel to PC surface at $z = 1.6$ μm (i.e., inside PC top layer), which corresponds to the maximum of BSW field distribution (see Figure 1c). The propagation of BSW at the particular angles is clearly observed. Then we calculated modes supported by a waveguide with the same cross-section as the

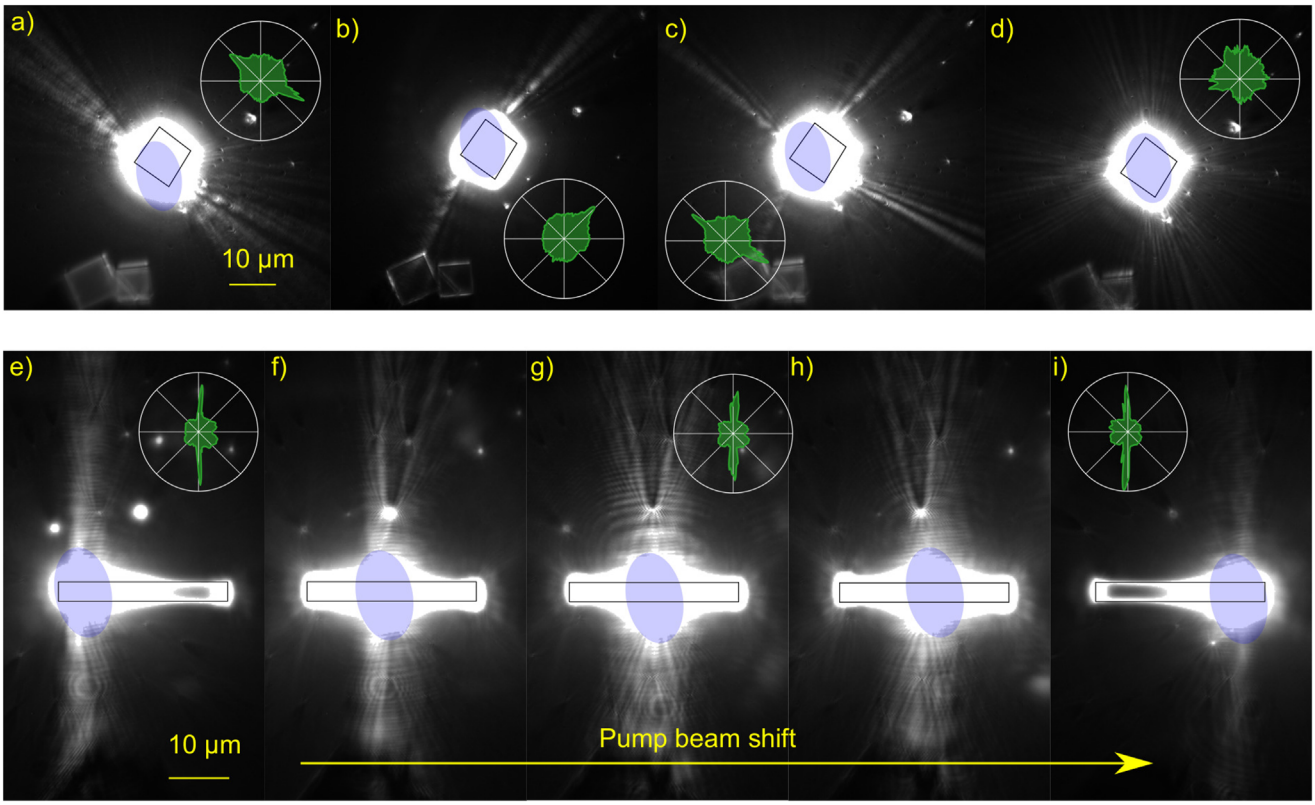

Figure 4. Microlaser coupling with Bloch surface waves. a–d) Visualization of the excited BSW for pump fluence above the lasing threshold for various pump beam positions. Borders of the microplate are shown with black line, position of pump beam is shown with blue ellipse. Insets show BSW directivity obtained from corresponding BFP images. e–h) FFP images of the BSW excited by emission of perovskite microwire with pump fluence above the lasing threshold for various pump beam positions. Insets show BSW directivity obtained from corresponding BFP images.

nanowire. The waveguide mode with similar field distribution has $n_{\text{eff}} = 1.73$ and provides similar spectrum and radiation directions (see Section S4, Supporting Information), that confirms the excitation of this particular mode in the case of lasing. We have also performed the same analysis for the nanowire placed on the ITO surface (see Section S6, Supporting Information). The spectrum of modes supported by the nanowire is similar to the spectrum in Figure 3a proving the absence of PC influence on the nanowire modes.

We also numerically estimated the efficiency of BSW excitation by the nanowire (see Section S7, Supporting Information for details). The obtained value of efficiency is 16% for dipole cloud excitation. This value is the lower estimation, since not all dipoles effectively participate in the excitation of the desired nanowire mode. The upper estimation can be obtained using a mode source, which is more suitable for efficient excitation of the nanowire lasing mode. In this case coupling efficiency appears to be around 30%. Thus, from 16% to 30% of the perovskite luminescence energy is involved in the BSW excitation. The obtained efficiencies are several times higher than similar values for coupling perovskite microlasers with other waveguides systems based on GaP,[27] Si_3N_4,[26] and plasmonic[28] waveguides. The demonstrated values for single mode lasers, including semiconductor ones,[40] usually do not exceed units of percent. The maximum efficiency of coupling between microlaser and waveguide has been observed in the system consisting of semiconductor nanowire lasers and silicon waveguide and was 16%.[41] Thus, the efficiency achievable by combining the perovskite microlaser with BSW platform is comparable or exceeds those described earlier. It is worth noting that the obtained efficiency depends on the PC parameters and can be increased by further structure optimization.

2.3. Steering of Bloch Surface Waves

The generation of laser radiation is achieved by creating an inverse population in the material due to external illumination. Sufficiently large perovskite structures sustain several modes, so it is possible to achieve the effective losses compensation for specific mode, while for the rest they remain significant and prevent the lasing. Thus, we can choose the lasing mode and, consequently, the direction of BSW excitation. **Figure 4**a–d shows switching of the BSW direction for a microplate with a size of 9 μm × 8 μm. The pump light locally injects electrons into conduction band and the modes located in pumped area have growing quality factor and start lasing under sufficient fluence. One or two modes separated in spectrum (see Section S8, Supporting Information) can be excited depending on the pump beam position that leads to one or two directions of BSW excitation (Figure 4a–c). Omnidirectional BSW generation is observed for beam position symmetrical relatively to the microplate (Figure 4d) or for

sufficiently high fluence (Figure S11, Supporting Information). This behavior is explained by the excitation of quasi-whispering gallery modes.

Another appealing possibility of BSW direction tuning is shifting of BSW beam with the pump beam movement along the wide microwire. If the wide microwire supports one or several modes across the long dimension, these modes can be excited locally only in the neighborhood with the pump beam position. Consequently, we can tune generated BSW beam with the pump beam shift (Figure 4e–i shows an example of microwire with a width of 2.1 μm). This property is useful for switching between waveguides located near the microwire. We estimate the divergence angle of generated BSW for such microwire as half-width at the half maximum of the directivity (directivity is shown in insets of Figure 4e,g,i). The divergence angle is $\theta = 9\pm2°$, that corresponds to numerical aperture of NA=$n_{BSW} \sin\theta = 0.17\pm0.05$. We also estimate BSW propagation length from FFP images Figure 4e–i. The value obtained from exponential fitting of the intensity along BSW propagation direction is 50±1 μm. Numerically estimated value of BSW propagation length at $\lambda = 535$ nm is 78.7 μm. Discrepancy is related to the scattering of BSW on the PC surface roughness and products of perovskite fabrication. Optimization of PC parameters can increase BSW propagation length (see Section S9, Supporting Information) and even widen BSW spectral range to the region from $\lambda = 300$ nm to $\lambda = 680$ nm. In this work, we choose slightly unoptimized PC (i.e., with higher losses) for the simplicity and clarity of the leakage radiation microscopy experimental results.

3. Discussion

Generally, the BSW platform possesses several advantages over conventional slab waveguides or metals supporting surface plasmon–polaritons. Fist of all, the PC layers can be made of various materials including semiconductors, oxides, magnetic or organic materials,[34,42–44] allowing for creation of substrates with unique multi-functional properties. Second, optimization of PC parameters leads to a superior light confinement and enhancement,[45] where the position of BSW field maximum can be arbitrary tuned inside the top layer of PC and adjusted to the PC–air interface. This opens up new possibilities of using the BSW platform in sensing[46] or optical trapping,[47] as well as for enhancing the interaction of light with the materials, which can be easily integrated with the BSW platform, for example, various ultra-thin 2D materials[48–50] with high optical nonlinearities[51–54] and supporting exciton-polaritons at room temperature.[50,55] Moreover, $CsPbBr_3$-based nano- and microlasers chemically tuned in broad spectral range[27,56] are prospective for spectrally adjusted in-plane irradiation of the various objects and materials on PC surface. This tunability fits perfectly with spectral flexibility of the BSW platform working in the visible and near-IR range.

To conclude, we have demonstrated the integration of halide perovskite nano- and microlasers with the platform based on 1D PC supporting efficient excitation and long-range propagation of BSW. The proposed PC hold lasing threshold of the halide perovskite lasers, but enables directional coherent emission outcoupling into BSWs with propagation length of 50 μm. The outcoupling through subwavelength facets of a perovskite nanowire forms a 2D interference pattern with domination of two beams from each side. Our experimental results agree well with full-wave numerical calculations, which provide the efficiency of lasing mode conversion into BSW over 16%. We also show that the BSW directivity depends on the length of the nanowire laser and on the BSW effective refractive index. In contrast to the perovskite nanolasers with subwavelength dimensions, perovskite microlasers with the facets much larger than the emitted wavelength support highly directional BSW with divergence angle of 9±2°. Moreover, in-plane isotropic dispersion law of BSW allows for the beam's shifting and steering by tuning the position of pump beam on the microlaser.

In the future, the proposed platform can be also suitable for the other applications. We envision future development toward integration of the nano- and microlasers made of various materials with on-chip optical elements (interferometers, modulators, resonators, etc.) empowered by the efficient coupling of laser modes to BSWs and their directional propagation over extremely long distances.

4. Experimental Section

Photonic Crystal Design: PC consisted of 6 pairs of SiO_2 (n_{SiO_2}=1.48 at λ=530 nm)/Ta_2O_5 ($n_{Ta_2O_5}$=2.12) alternating layers with thicknesses of 143 and 101 nm, respectively, deposited on a 170-μm-thick glass substrate (n_{sb}=1.52) by physical vapor deposition technique. The top layer was SiO_2. PC was designed to sustain TE-polarized BSW in a wide spectral range from 450 to 650 nm (see Section S1, Supporting Information), where n_{BSW} changes from 1.27 to 1.

Perovskite Nanowires and Microplates Fabrication: Single-crystal $CsPbBr_3$ nano- and microcavities were synthesized by using a protocol that was similar to the earlier reported one.[17] Perovskite precursors lead (II) bromide ($PbBr_2$, Alfa Aesar, 99.998 %) and cesium(I) bromide (CsBr, Sigma-Aldrich, 99.999%) were mixed as 0.105:0.100 mmol, respectively, and dissolved in 1 mL of anhydrous dimethyl sulfoxide (DMSO, Sigma-Aldrich, 99.9%) in a N_2-filled glovebox with both oxygen and moisture levels not exceeding 1 ppm. A small excess of $PbBr_2$ (0.005 mmol) added to the precursors solution (perovskite ink) prevented the crystallization of the Cs_4PbBr_6 phase doped with $CsPbBr_3$ quantum dots showing parasitic blue photoluminescence. 5 μL of the obtained clear solution was drop-casted on the PC at ambient conditions. Thereafter, the substrate with the droplet was sealed in a hot glass Petri dish (100 mL) containing 200 μL of water-2-propanol azeotropic mixture and kept at 60 °C for 5 min until the droplet was completely dry. During this procedure, the azeotropic vapor condensed on the outside of the deposited droplet and substantially increased its volume. As a result, the droplet spreaded out over the whole surface of the PC. Since 2-propanol does not dissolve perovskite and facilitates the volatilization of DMSO, the regions oversaturated with the precursors were formed in the mixture of 2-propanol and perovskite ink. The latter resulted in rapid crystallization of $CsPbBr_3$ microcavities and their precipitation on the surface of the PC. A comparison of Raman spectra from perovskite nanowires grown on PC and SiO_2 glass substrate did not reveal considerable difference (Section S10, Supporting Information).

Leakage Radiation Microscopy: Coupling of BSW and lasing radiation of perovskite microstructures was studied using leakage radiation microscopy (LRM). LRM allowed visualizing the BSW field and wavevector distribution. The output radiation from Ti:sapphire femtosecond laser (Coherent Chameleon Ultra II, λ_p=800 nm, 150 fs pulse duration, 80 MHz repetition rate) passed through the pulse picker (Avesta OG-B, 7 ns rise time, 1000:1 contrast) to reduce the repetition rate down to 50 kHz. After that the laser radiation pumped a custom second-harmonic generator. Then second harmonic was focused by a lens on the PC surface into a spot 9.5 μm × 15 μm in size. The precise position of the sample was con-

trolled by the three-axis motorized stage. Leakage radiation was collected using an oil-immersion objective lens with high numerical aperture (NA= 1.3, 100×, Olympus UPLFLN100XOI2). The collected light passed through a filtering system, which constructed intermediate FFP and BFP images of the collecting objective lens. Filtering was performed with an aperture and/or nontransparent round block located in the intermediate FFP and BFP images, respectively. After filtering, the FFP or BFP image was constructed on the sensor of CMOS cameras (Thorlabs CS2100-USB) which allowed obtaining BSW field and wavevector distribution. The additional information on LRM setup is provided in Section S2, Supporting Information.

Supporting Information

Supporting Information is available from the Wiley Online Library or from the author.

Acknowledgements

K.R.S. and A.A.P. contributed equally to this work. The authors thank I. M. Antropov and V. A. Sitnyansky for sample characterization (AFM and SEM). The work was performed under partial financial support of the Russian Ministry of Education and Science (Grant No. 14.W03.31.0008), the Russian Science Foundation (Grant No. 20-12-00371). Part of the research was supported by MSU Quantum Technology Center and the MSU Interdisciplinary Scientific and Educational School "Photonic and Quantum technologies. Digital Medicine." S.V.M. and A.P.P acknowledge the Ministry of Science and Higher Education of the Russian Federation (Project No. 075-15-2021-589). The work was partially done in ITMO Core Facility Center "Nanotechnologies."

Conflict of Interest

The authors declare no conflict of interest.

Data Availability Statement

The data that support the findings of this study are available in Supporting Information of this article.

Keywords

Bloch surface waves, halide perovskites, integrated photonics, microlasers, nanolasers, nanowires

Received: December 24, 2021
Revised: February 21, 2022
Published online: March 31, 2022

[1] C. Sun, M. T. Wade, Y. Lee, J. S. Orcutt, L. Alloatti, M. S. Georgas, A. S. Waterman, J. M. Shainline, R. R. Avizienis, S. Lin, B. R. Moss, R. Kumar, F. Pavanello, A. H. Atabaki, H. M. Cook, A. J. Ou, J. C. Leu, Y.-H. Chen, K. Asanović, R. J. Ram, M. A. Popović, V. M. Stojanović, *Nature* **2015**, *528*, 534.
[2] J. B. Spring, B. J. Metcalf, P. C. Humphreys, W. S. Kolthammer, X.-M. Jin, M. Barbieri, A. Datta, N. Thomas-Peter, N. K. Langford, D. Kundys, J. C. Gates, B. J. Smith, P. G. R. Smith, I. A. Walmsley, *Science* **2013**, *339*, 798.
[3] J. Leuthold, C. Koos, W. Freude, *Nat. Photonics* **2010**, *4*, 535.
[4] I. Aharonovich, D. Englund, M. Toth, *Nat. Photonics* **2016**, *10*, 631.
[5] I. Aharonovich, E. Neu, *Adv. Opt. Mater.* **2014**, *2*, 911.
[6] G. Xing, N. Mathews, S. S. Lim, N. Yantara, X. Liu, D. Sabba, M. Grätzel, S. Mhaisalkar, T. C. Sum, *Nat. Mater.* **2014**, *13*, 476.
[7] Q. Zhang, S. T. Ha, X. Liu, T. C. Sum, Q. Xiong, *Nano Lett.* **2014**, *14*, 5995.
[8] F. Deschler, M. Price, S. Pathak, L. E. Klintberg, D.-D. Jarausch, R. Higler, S. Hüttner, T. Leijtens, S. D. Stranks, H. J. Snaith, M. Atatüre, R. T. Phillips, R. H. Friend, *J. Phys. Chem. Lett.* **2014**, *5*, 1421.
[9] H. Zhu, Y. Fu, F. Meng, X. Wu, Z. Gong, Q. Ding, M. V. Gustafsson, M. T. Trinh, S. Jin, X. Zhu, *Nat. Mater.* **2015**, *14*, 636.
[10] S. W. Eaton, M. Lai, N. A. Gibson, A. B. Wong, L. Dou, J. Ma, L.-W. Wang, S. R. Leone, P. Yang, *Proc. Natl. Acad. Sci. U. S. A.* **2016**, *113*, 1993.
[11] Y. Fu, H. Zhu, C. C. Stoumpos, Q. Ding, J. Wang, M. G. Kanatzidis, X. Zhu, S. Jin, *ACS Nano* **2016**, *10*, 7963.
[12] Y. Wang, X. Sun, R. Shivanna, Y. Yang, Z. Chen, Y. Guo, G.-C. Wang, E. Wertz, F. Deschler, Z. Cai, H. Zhou, T.-M. Lu, J. Shi, *Nano Lett.* **2016**, *16*, 7974.
[13] H. Zhou, S. Yuan, X. Wang, T. Xu, X. Wang, H. Li, W. Zheng, P. Fan, Y. Li, L. Sun, A. Pan, *ACS Nano* **2017**, *11*, 1189.
[14] Q. Zhang, R. Su, W. Du, X. Liu, L. Zhao, S. T. Ha, Q. Xiong, *Small Methods* **2017**, *1*, 1700163.
[15] B. Tang, H. Dong, L. Sun, W. Zheng, Q. Wang, F. Sun, X. Jiang, A. Pan, L. Zhang, *ACS Nano* **2017**, *11*, 10681.
[16] K. Wang, S. Wang, S. Xiao, Q. Song, *Adv. Opt. Mater.* **2018**, *6*, 1800278.
[17] A. P. Pushkarev, V. I. Korolev, D. I. Markina, F. E. Komissarenko, A. Naujokaitis, A. Drabavicius, V. Pakstas, M. Franckevicius, S. A. Khubezhov, D. A. Sannikov, S. Makarov, *ACS Appl. Mater. Interfaces* **2019**, *11*, 1040.
[18] E. Y. Tiguntseva, K. L. Koshelev, A. D. Furasova, P. Tonkaev, V. Y. Mikhailovskii, E. V. Ushakova, D. G. Baranov, T. O. Shegai, A. A. Zakhidov, Y. S. Kivshar, S. V. Makarov, *ACS Nano* **2020**, *14*, 8149.
[19] L. Zhao, Y. Gao, M. Su, Q. Shang, Z. Liu, Q. Li, Q. Wei, M. Li, L. Fu, Y. Zhong, J. Shi, J. Chen, Y. Zhao, X. Qiu, X. Liu, N. Tang, G. Xing, X. Wang, B. Shen, Q. Zhang, *ACS Nano* **2019**, *13*, 10085.
[20] Y. Fu, H. Zhu, J. Chen, M. P. Hautzinger, X.-Y. Zhu, S. Jin, *Nat. Rev. Mater.* **2019**, *4*, 169.
[21] Q. Zhang, Q. Shang, R. Su, T. T. H. Do, Q. Xiong, *Nano Lett.* **2021**, *21*, 1903.
[22] S. H. Lee, D. Y. Oh, Q.-F. Yang, B. Shen, H. Wang, K. Y. Yang, Y.-H. Lai, X. Yi, X. Li, K. Vahala, *Nat. Commun.* **2017**, *8*, 1295.
[23] S. Romero-García, F. Merget, F. Zhong, H. Finkelstein, J. Witzens, *Opt. Express* **2013**, *21*, 14036.
[24] M. J. Burek, Y. Chu, M. S. Liddy, P. Patel, J. Rochman, S. Meesala, W. Hong, Q. Quan, M. D. Lukin, M. Lončar, *Nat. Commun.* **2014**, *5*, 5718.
[25] D. J. Wilson, K. Schneider, S. Hönl, M. Anderson, Y. Baumgartner, L. Czornomaz, T. J. Kippenberg, P. Seidler, *Nat. Photonics* **2020**, *14*, 57.
[26] P. Cegielski, A. L. Giesecke, S. Neutzner, C. Porschatis, M. Gandini, D. Schall, C. Perini, J. Bolten, S. Suckow, S. Kataria, B. Chmielak, T. Wahlbrink, A. Petrozza, M. Lemme, *Nano Lett.* **2018**, *18*, 6915.
[27] P. Trofimov, A. P. Pushkarev, I. S. Sinev, V. V. Fedorov, S. Bruyere, A. Bolshakov, I. S. Mukhin, S. V. Makarov, *ACS Nano* **2020**, *14*, 8126.
[28] Y. J. Li, Y. Lv, C.-L. Zou, W. Zhang, J. Yao, Y. S. Zhao, *J. Am. Chem. Soc.* **2016**, *138*, 2122.
[29] R. Dubey, E. Barakat, M. Häyrinen, M. Roussey, S. K. Honkanen, M. Kuittinen, H. P. Herzig, *J. Eur. Opt. Soc.-Rapid Publ.* **2017**, *13*, 5.
[30] T. Perani, M. Liscidini, *Opt Lett.* **2020**, *45*, 6534.
[31] H. Luo, X. Tang, Y. Lu, P. Wang, *Phys. Rev. Appl.* **2021**, *16*, 014064.
[32] R. Su, J. Wang, J. Zhao, J. Xing, W. Zhao, C. Diederichs, T. C. Liew, Q. Xiong, *Sci. Adv.* **2018**, *4*, eaau0244.

[33] E. Descrovi, E. Barakat, A. Angelini, P. Munzert, N. De Leo, L. Boarino, F. Giorgis, H. P. Herzig, *Opt. Lett.* **2013**, *38*, 3374.
[34] K. R. Safronov, D. N. Gulkin, I. M. Antropov, K. A. Abrashitova, V. O. Bessonov, A. A. Fedyanin, *ACS Nano* **2020**, *14*, 10428.
[35] P. Yeh, A. Yariv, C.-S. Hong, *J. Opt. Soc. Am.* **1977**, *67*, 423.
[36] A. S. Polushkin, E. Y. Tiguntseva, A. P. Pushkarev, S. V. Makarov, *Nanophotonics* **2020**, *9*, 599.
[37] D. I. Markina, A. P. Pushkarev, I. I. Shishkin, F. E. Komissarenko, A. S. Berestennikov, A. S. Pavluchenko, I. P. Smirnova, L. K. Markov, M. Vengris, A. A. Zakhidov, S. V. Makarov, *Nanophotonics* **2020**, *9*, 3977.
[38] A. Angelini, E. Barakat, P. Munzert, L. Boarino, N. De Leo, E. Enrico, F. Giorgis, H. P. Herzig, C. F. Pirri, E. Descrovi, *Sci. Rep.* **2014**, *4*, 5428.
[39] D. Saxena, F. Wang, Q. Gao, S. Mokkapati, H. H. Tan, C. Jagadish, *Nano Lett.* **2015**, *15*, 5342.
[40] D. Jevtics, A. Hurtado, B. Guilhabert, J. McPhillimy, G. Cantarella, Q. Gao, H. H. Tan, C. Jagadish, M. J. Strain, M. D. Dawson, *Nano Lett.* **2017**, *17*, 5990.
[41] T. Stettner, T. Kostenbader, D. Ruhstorfer, J. Bissinger, H. Riedl, M. Kaniber, G. Koblmüller, J. Finley, *ACS Photonics* **2017**, *4*, 2537.
[42] M. Liscidini, D. Gerace, D. Sanvitto, D. Bajoni, *Appl. Phys. Lett.* **2011**, *98*, 121118.
[43] M. N. Romodina, I. V. Soboleva, A. I. Musorin, Y. Nakamura, M. Inoue, A. A. Fedyanin, *Phys. Rev. B* **2017**, *96*, 081401.
[44] G. Lerario, D. Ballarini, A. Fieramosca, A. Cannavale, A. Genco, F. Mangione, S. Gambino, L. Dominici, M. De Giorgi, G. Gigli, D. Sanvitto, *Light Sci. Appl.* **2017**, *6*, e16212.
[45] D. Aurelio, M. Liscidini, *Phys. Rev. B* **2017**, *96*, 045308.
[46] Y. Kuai, J. Chen, X. Tang, Y. Xiang, F. Lu, C. Kuang, L. Xu, W. Shen, J. Cheng, H. Gui, G. Zou, P. Wang, H. Ming, J. Liu, X. Liu, J. R. Lakowicz, D. Zhang, *Sci. Adv.* **2019**, *5*, eaav5335.
[47] D. A. Shilkin, E. V. Lyubin, I. V. Soboleva, A. A. Fedyanin, *Opt. Lett.* **2015**, *40*, 4883.
[48] B. Zhu, X. Chen, X. Cui, *Sci. Rep.* **2015**, *5*, 9218.
[49] H. Zhao, Q. Guo, F. Xia, H. Wang, *Nanophotonics* **2015**, *4*, 128.
[50] T. Low, A. Chaves, J. D. Caldwell, A. Kumar, N. X. Fang, P. Avouris, T. F. Heinz, F. Guinea, L. Martin-Moreno, F. Koppens, *Nat. Mater.* **2017**, *16*, 182.
[51] R. Woodward, R. Murray, C. Phelan, R. De Oliveira, T. Runcorn, E. Kelleher, S. Li, E. De Oliveira, G. Fechine, G. Eda, C. J. S. de Matos, *2D Mater.* **2016**, *4*, 011006.
[52] A. A. Popkova, I. M. Antropov, J. E. Fröch, S. Kim, I. Aharonovich, V. O. Bessonov, A. S. Solntsev, A. A. Fedyanin, *ACS Photonics* **2021**, *8*, 824.
[53] C. Janisch, Y. Wang, D. Ma, N. Mehta, A. L. Elías, N. Perea-López, M. Terrones, V. Crespi, Z. Liu, *Sci. Rep.* **2014**, *4*, 5530.
[54] Q. Guo, Z. Ou, J. Tang, J. Zhang, F. Lu, K. Wu, D. Zhang, S. Zhang, H. Xu, *Nano Lett.* **2020**, *20*, 7956.
[55] V. Ardizzone, L. De Marco, M. De Giorgi, L. Dominici, D. Ballarini, D. Sanvitto, *Nanophotonics* **2019**, *8*, 1547.
[56] S. Makarov, A. Furasova, E. Tiguntseva, A. Hemmetter, A. Berestennikov, A. Pushkarev, A. Zakhidov, Y. Kivshar, *Adv. Opt. Mater.* **2019**, *7*, 1800784.